Design of an ultralight and compact projection lens

Hong Hua, Yonggang Ha, and Jannick P. Rolland

Driven by the need for lightweight head-mounted displays, we present the design of an ultralight and compact projection lens for a head-mounted projective display (HMPD). An HMPD consists of a pair of miniature projection lenses, beam splitters, and miniature displays mounted on the helmet and retroreflective sheeting materials placed strategically in the environment. The HMPD has been proposed recently as an alternative modality for three-dimensional visualization. After demonstrating the concept, building a first-generation custom-designed prototype, and investigating perception issues and application potentials, we designed an ultralight and compact projective lens with a diffractive optical element (DOE), plastic components, and aspheric surfaces for the next-generation prototype. The key contribution here lies in the conception, optimization, and assessment of the projection optics. Thus a brief review of the HMPD technology and related research is followed by a detail discussion of the conception and optimization of the ultralight and high-performance projection optics. The design of the DOE will be particularly described in detail. Finally, the diffraction efficiency of the DOE will be evaluated, and the overall performance of the optics will be assessed in both object space for the optical designer and visual space for possible end-users of the technology.

OCIS codes: 050.1970, 080.2740, 080.3620, 120.2820, 220.0220, 230.3990.

1. Introduction

Head-mounted displays (HMDs) have been widely used for three-dimensional (3D) visualization tasks such as surgical planning, medical training, or engineering design.[1] The main issues of the conventional eyepiece-based HMD technology include the trade-offs between resolution and field of view (FOV) as well as between compactness and eye clearance, the presence of great distortion for wide FOV designs, the conflict of accommodation and convergence, the occlusion contradiction between virtual and real objects, the challenge of highly precise registration, and often the brightness conflict with bright background illumination.[2–5] The concept of head-mounted projective displays (HMPDs) is an emerging technology that can be thought to lie on the boundary of conventional HMDs and projective displays such as the CAVE (computer-automated virtual environment) technology.[6–10] The concept has been recently demonstrated to yield 3D visualization capability with a large FOV (i.e., ~70 deg with a flat retroreflective screen based on current materials), lightweight optics, low distortion, and the correct occlusion of virtual objects by real objects.[11,12] Thus the technology is being developed and tested by a few research groups as an alternative to stereoscopic displays for a variety of 3D visualization applications.[13–17]

We have designed a pair of projection lenses for the HMPD by using the combination of a diffractive optical element (DOE), plastic components, and aspheric surfaces, achieving a 52-deg FOV with a weight of only 8 g and a 15 mm diameter × 20 mm long lens. In this paper we present the conception, optimization, and assessment of ultralight and compact projection optics. We first review the HMPD technology and related research before presenting the conception and optimization of the ultralight and high-performance projection optics. The design of the DOE is especially described in detail, its diffraction efficiency evaluated, and the overall performance of the optics assessed in both the space of the miniature flat panel display and visual space in order to provide useful metrics for the end-users of the technology as well.

2. Overview of the HMPD Technology

An HMPD, conceptually illustrated in Fig. 1, consists of a pair of miniature projection lenses, beam split-

H. Hua is with Beckman Institute, University of Illinois Urbana-Champaign, Urbana, Illinois 61801 (e-mail, Honghua@uiuc.edu). The other authors are with the School of Optics, Center for Research and Education in Optics and Lasers, University of Central Florida, Orlando, Florida 32816 (e-mail for J. Rolland, Jannick@odalab.ucf.edu).

Received 27 December 2001; revised manuscript received 11 April 2002.

0003-6935/03/010097-11$15.00/0

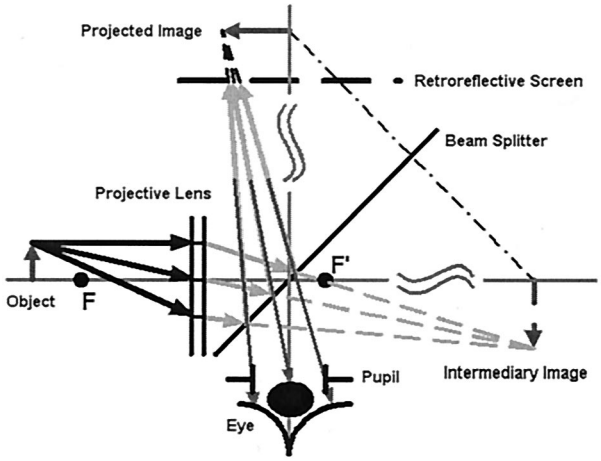

Fig. 1. Imaging concept of HMPDs.

ters, miniature displays mounted on the head, and a supple and nondistorting retroreflective sheeting material placed strategically in the environment.[6,7,11] An image on the miniature display is projected through the lens as a real image and retroreflected back to the entrance pupil of the eye, where the exit pupil of the optics (i.e., the projection lens plus the beam splitter) is located. Because of the retroreflective property illustrated in Fig. 2 in which the rays hitting the surface are reflected back on themselves in the opposite direction, the location and size of the perceived image are theoretically independent of the location and shape of the retroreflective screen. In practice, however, imperfect retroreflection leads to degradation in the imaging quality when the screen is far from the nominal distance or reduction in image brightness when the screen is significantly curved.[11]

A. HMPD Technology Highlights

Two major aspects distinguish the HMPD technology from conventional HMDs and stereoscopic projection systems: Projection optics instead of eyepiece optics is at the heart of the imaging, and a retroreflective screen instead of a diffusing screen is employed.[10,12] Unique to the technology is the property of the technology that provides an optical see-through capability in spite of the screen. The see-through capability allows optical augmentation of the real world with computer-generated objects. The HMPD technology also provides intrinsically correct occlusion of computer-generated virtual objects by real objects, as demonstrated in Fig. 3. Furthermore the technology creates a ubiquitous display environment in which the retroreflective material can be applied anywhere in physical space and can be tailored to

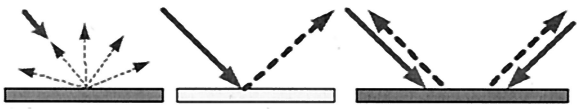

Fig. 2. Behavior of different reflective surfaces: (a) diffusing surface, (b) reflective surface, (c) retroreflective surface.

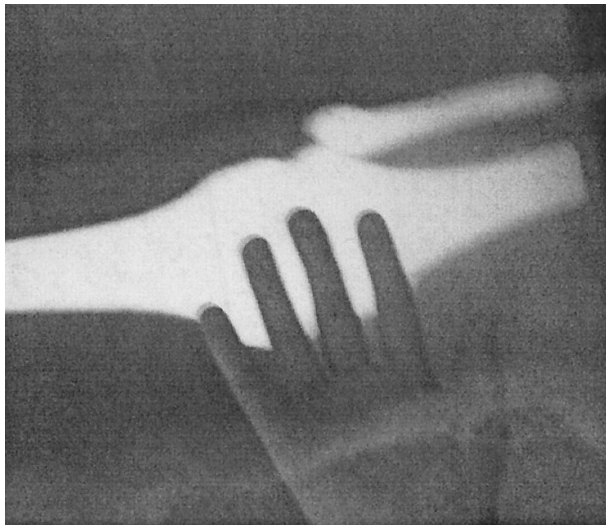

Fig. 3. Natural occlusion of computer-generated object (bone) by real object (hand) in HMPD. Such occlusion is not achievable in conventional see-through displays.

arbitrary shapes without introducing additional distortion to the virtual images. Finally the technology can support unique perspectives for each participant in a multiple-user collaborative environment without introducing cross talk from other participants.[12,15,16] Moreover, compared with conventional eyepiece-based optical see-through HMDs, utilization of projective optics allows for reduced optical distortion across similar FOVs. Finally projection optics better meets the pupil-size and eye-relief requirements.

B. Previous Research

The basic HMPD concept was first presented by Kijima and Ojika in 1997,[6] while a patent was also issued on the conceptual idea of the display to Fergason in 1997.[7] Tachi *et al.* developed a configuration called X'tal Vision and proposed the concept of object-oriented display and visual-haptic display.[14,17] Independently the technology of HMPD was developed by Parsons and co-workers as a tool for medical visualization.[9,18] After the initial proof of concept, using off-the-shelf components, we built a first-generation custom-designed HMPD prototype to investigate perception issues and quantify some of the properties and behaviors of the retroreflective materials in imaging systems.[10] We are currently investigating various applications of the HMPD technology in distance collaborative augmented environments.[13,15,16]

The first-generation prototype was custom-designed with a double-Gauss lens form built with commercially available components.[11] The effective focal lens of the optics was 22.2 mm, and it provided an ~40-deg diagonal FOV. The total weight of each lens assembly was ~50 g. An already significant reduction was compared with off-the-shelf optics; the mechanical dimensions of the optics were 35 mm in length by 43 mm in diameter. The modulation transfer function (MTF) achieved ~20% transmission at 20 lp/mm.

3. Design of an Ultralight and Compact Head-mounted Projection Optics

Lightweight and compactness are always highly desirable for head-mounted devices. Based on the first-generation prototype, further efforts have been made to design an ultralight projection system with a combination of the DOE, plastic components, and aspheric surfaces. In this section we focus on design specifications and conception.

A. Overall Specifications

When a flat combiner is used (i.e., a beam splitter), only the projection optics needs to be designed. The miniature display selected based on availability and cost was 1.35 in. (3.4-cm) backlighting color AMLCDs (active-matrix LCDs) with (640 × 3) × 480 pixels and a 42-μm pixel size. Given the miniature display, a wide FOV and high resolution are always two contradictory but desirable requirements.[19] Besides the consideration of resolution, there are two limitations on the targeted FOV. One is that using a flat beam splitter gives a maximum FOV of 90 deg. The other is the significant retroreflectivity drop-off of currently available retroreflective materials beyond ±35° deg of incidence, which imposes an upper limit of 70 deg on the FOV for a flat retroreflective screen.[10,15] Therefore, given the resolution of the flat panel display available for this design, a diagonal FOV between 50 and 55 deg, which corresponds to 36.9–33.1 mm of focal length, is preferred. We thus decided on a 35-mm focal length yielding a precise 52.4-deg FOV.

In the design of visual instruments, especially binocular HMDs, it is necessary to account for the eyes of the wearers swiveling in their sockets; such swiveling causes the pupil to be displaced relative to the optical system. This requirement becomes more critical for a pupil-forming system such as the HMPD. As a result the exit pupil size is specified to be 12 mm although the diameter of the eye pupil is typically 3–5 mm in the lighting conditions provided by the HMD. Such a pupil-size specification allows a swivel of ±25° without causing vignetting with a 3-mm-eye pupil. Furthermore it allows a ±6-mm interpupilary distance (IPD) tolerance for different users when the IPD is not set precisely.[20] For applications where the accuracy of rendered depth is critical, however, the IPD between the two arms of the optics should be set to the IPD of the user and the setting should be reflected in the computational model to display stereoscopic images. In terms of performance evaluation, 12-mm and 3-mm pupils are assessed in the miniature-display space and visual space, respectively.

An effective eye clearance of 23 mm is necessary to allow for all types of eyeglasses.[21] It is always a design constraint for eyepiece-type HMDs because the optics size and therefore the weight scales directly with the increase in FOV. However, it is not a direct limitation in the HMPD because the eye clearance can be adjusted to the required specification by simply adjusting the separation between the projection lens and the beam splitter.

Table 1. Optical Design Specification

Parameter	Specification
Object: Color LCD	
Size	1.35 in (3.42 cm) diagonally
Active display area	Rectangle, 26.4 mm × 19.8 mm
Resolution	(640 × 3) × 480 pixels
Lens	
Type	Projection lens
Effective focal length	35 mm
Exit pupil diameter	12 mm
Eye relief	25 mm
Number of diffractive surfaces	1
Number of aspheric surfaces	1
Other parameters	
Wavelength range	656–486 nm
FOV	52.4° diagonally
Distortion	<2.5% over entire FOV

Optical-system aberrations may cause either a decrease in image sharpness (i.e., spherical aberration, coma, field curvature, and astigmatism) or warping of the image (i.e., distortion), the latter allowing computational or electronic correction. In conventional HMD designs it is common to optimize the design with respect to the optical aberrations that cannot be compensated for electronically or computationally.[3] In the case of projection optics the location of the pupil within the lens naturally calls for low distortion. Therefore all primary aberrations are minimized in the HMPD. The optical specification of the projection lens is summarized in Table 1.

B. Conception of an Ultralight and Compact Design

Most of the LCD-based projection systems are designed to be telecentric to achieve uniform illumination. Although uniform illumination is desirable, it requires that the lens aperture be at least the same size as the display device. Because compactness is a critical factor in HMDs, we relaxed the telecentric constraint to gain compactness.

Furthermore an established effective way to design an ultralight, compact, and high-quality lens is to use a combination of plastic components and DOEs.[22] In the design of large-aperture projection systems, DOEs may be applied to correct the secondary spectrum and residual spherical aberrations for apochromatic imaging in place of using high-index lanthanum crown glasses.[23–25] The advantages of using DOEs over conventional refractive optics lie in their capability of designing large-aperture and lightweight optical elements, achieving aspheric-like aberration correction, obtaining achromatization in combination with refractive elements, eliminating the need for exotic materials, gaining performance over conventional systems, and significantly reducing system complexity and cost.[26–29]

With these considerations for head-mounted applications, our goal was to achieve a compact design

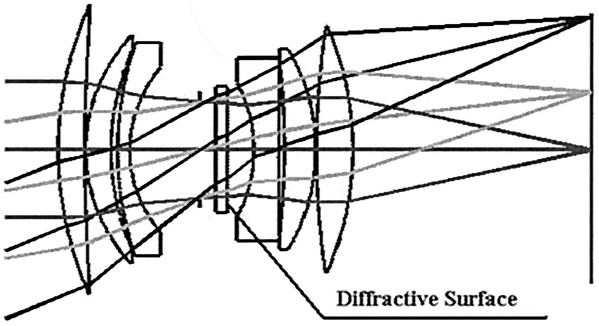

Fig. 4. Apochromatic double-Gauss, 51.75 mm, $F/1.46$), lens with a two-layer diffractive surface (U.S. patent 5,930,043).

with at least two glass components, a glass lens nearest to the eye and a glass lens nearest to the display to provide a robust seal for the optical module. The exposure of glass components in air, rather than plastic components, protects the system from oxidization, i.e., aging caused by the reaction of plastic with acid in the air, or scratches.

We used as a starting point to the design process a patented lens by Ogawa[23,24] that consists of a 51.75-mm $F/1.46$ apochromatic double-Gauss lens with a two-layer diffractive surface on a plane-parallel substrate. The layout of the lens is shown in Fig. 4. The second surface of the plate component has a replicated DOE. Its full FOV is 45.32°. To reduce the number of elements to four, the plate just after the aperture shown in Fig. 4, which had a DOE element, was removed from the original design. Then the resultant form was scaled to a 35-mm focal length with a 12-mm entrance pupil, and a few cycles of optimization were executed to increase the image size to 17.2 mm to account for the size of the LCD image source. This process led to an optimized double-Gauss scaled starting point shown in Fig. 5, and the polychromatic diffraction MTF shows acceptable performance as a starting point for the design.

Adopting a strategy of gradual simplification and accounting for the fact that a singlet lens with a DOE can replace the functions of a doublet, we replaced the first glass doublet (components 2 and 3 in Fig. 5) with a poly (methyl methacrylate) plastic singlet. The initial optimization was applied so that the second surface of the singlet was close to planar, which is recommended for replication of a DOE feature on the corresponding surface. A DOE feature with a spherical substrate was then designated to the second planar surface of the singlet. The design of the DOE is discussed in detail in Section 4. Further optimization was applied that led to a five-component design. The MTF maintained more than 40% at a 25-lp/mm resolution across the FOV, which led us to (further) simplify the design. The next step was to replace the second doublet (components 4 and 5 in Fig. 5) with a styrene plastic singlet with spherical surfaces. Initial optimization was applied to reach the initial four-element design format shown in Fig. 6. The main constraints that we utilized during the conceptual design included control of the effective focal length, field weights, and optical power on the DOE.

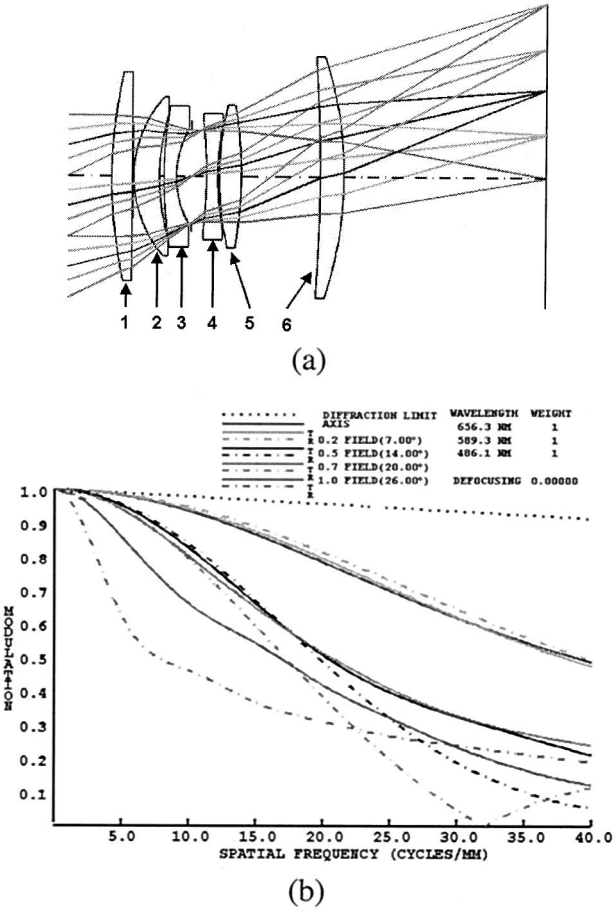

Fig. 5. Optimized starting point of a 35 mm, $F/2.9$ double-Gauss lens: (a) lens profile and (b) polychromatic MTF performance for a 12-mm pupil.

4. Design of the Diffractive Optical Element

In this section we concentrate on the DOE design including selection of physical forms, optical power, substrate, phase function, and depth profile for fabrication considerations.

Typically, there are four physical forms of DOEs: zone plate, binary optics, a photoetched multilevel DOE, and a kinoform DOE. We adopted the kinoform DOE because it is usually fabricated by diamond-turning techniques that can cut the substrate shape and the DOE profile at the same time.[26,27] Therefore the substrate shape of a kinoform DOE can be spherical, planar being a special case, or aspheric. Nonplanar substrates provide more flexibility on higher-order aberration correction with no increase in cost.

The commonly used diffractions are 0, +1, or −1. We adopted the +1 order of diffraction. The focal length of the DOE is given by

$$f = -0.5/c_q, \tag{1}$$

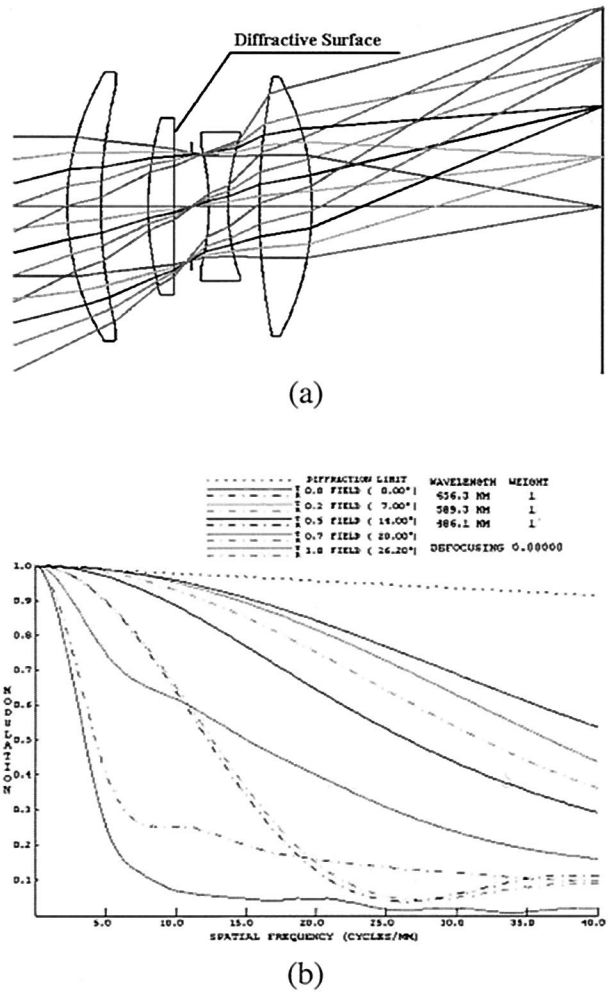

Fig. 6. Four-element, 35 mm, $F/2.9$ projection lens with a DOE surface and two plastic components: (a) lens profile and (b) polychromatic MTF performance for a 12-mm pupil.

where c_q is the quadratic phase coefficient of the DOE. DOEs can be viewed as a material with large dispersion but opposite in sign to conventional materials (i.e., the V number of a DOE is approximately -3.5 for the visible spectrum). For monochromatic applications the DOEs are typically designed to have significant optical power and can be viewed as replacements for refractive optics. However, for polychromatic applications, in which the HMPD application belongs, the DOEs are typically designed to have little optical power. During optimization c_q is constrained by setting $c_q \geq -0.001$. This one-sided constraint actually allows the DOE quadratic coefficient algebraically to be arbitrarily large (negative), which lets the focal length be as large (positive) as it wants to be. The main purpose of this constraint is to obtain achromatization in combination with refractive elements[26] and minimize spherochromatism. In the final design, $c_q = -0.0007319$, which corresponds to a focal length of 683.15 mm.

While the substrate of the kinoform can be spherical and aspheric, its curvature must be small enough for the fabrication of DOE features. The design further required an aspheric substrate that would correct the higher-order aberrations in a four-element system. The profile of the substrate is specified by the function $Z_4(h)$ given by

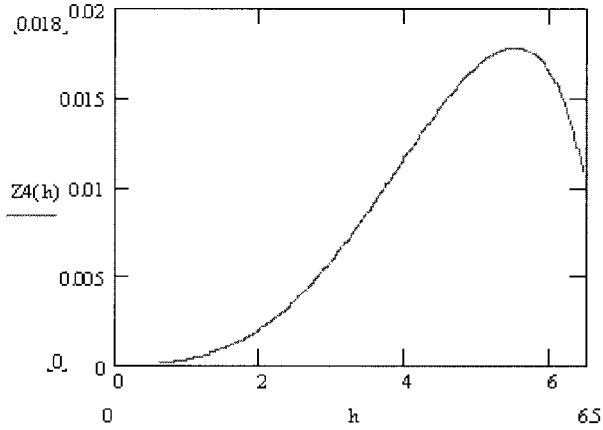

Fig. 7. Profile of the DOE substrate.

$$Z_4(h) = \frac{ch^2}{1 + [1 - (1 + k)c^2h^2]^{1/2}} + Ah^4 + Bh^6 + Ch^8 + Dh^{10}. \quad (2)$$

Coefficients k, c, A, B, C, and D were initialized to zero and were made to be variables during the optimization. In the final design $k = 0.1909845e^{-4}$, $c = 5.5548e^{-4}$, $A = 0.68758e^{-4}$, $B = -0.3534475e^{-5}$, $C = 0.7411626e^{-7}$, and $D = -0.70094e^{-9}$. The profile of the aspheric substrate is shown in Fig. 7.

The periodic grating feature of the DOE is defined by a phase function. A rotationally symmetric phase function ϕ is given by

$$\phi = \frac{2\pi}{\lambda_0} \sum_{i=1}^{M=6} c_i r^{2i} \quad (3)$$

where λ_0 is the designed wavelength (i.e., 550 nm in the design). Coefficients $c_i (i = 1 \ldots 6)$ were initialized to zero except for $c_q = c_q = -0.001$ and were assigned to be variables during the optimization. In the final design $c_1 = -0.00073188096$, $c_2 = -0.681429819273e^{-5}$, $c_3 = -0.110892752416e^{-6}$, $c_4 = 0.441029605345e^{-7}$, $c_5 = -0.158823366883e^{-8}$, and $c_6 = 0.165824784197e^{-10}$. The phase profile across the radius of the element is shown in Fig. 8. The phase change reached around 55 times the wavelength, leading to a maximum phase change of 55 times 2π.

For fabrication the phase function is transformed into a depth profile to define the feature parameters. The depth profile is given by

$$t(r) = \frac{\lambda_0}{2\pi(n_0 - 1)} (\phi \bmod 2\pi), \quad (4)$$

where t varies from 0 to $d = \lambda_0/(n_0 - 1)$ across the radius of the element, where d is the depth period of the grating features for the designed wavelength, or

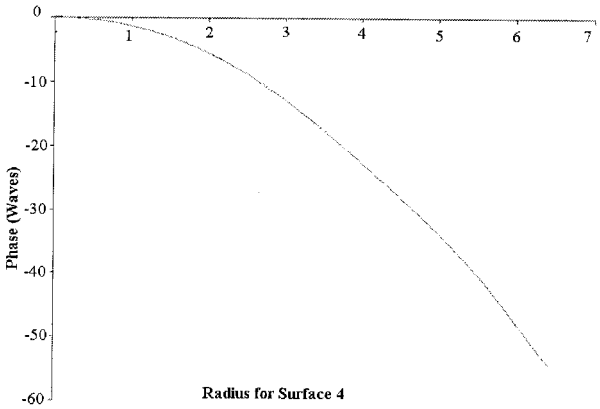

Fig. 8. Phase profile the DOE.

1.12 μm in the design. The DOE depth profile across the radius of the element is shown in Fig. 9(a). The DOE grating features can be specified by the feature depth d, the radii of the zone transitions r, the size of the zones Δr, and the number of zones N, as illustrated in Fig. 9 (b). The radii of the zone transitions r_m and the number of zones N are computed as

$$m\lambda_0 = \sum_{i=1}^{6} c_i {r_m}^{2i} \ (m = 1, 2, \ldots, N), \tag{5}$$

$$N = \frac{1}{\lambda_0} \sum_{i=1}^{6} c_i {r_{\max}}^{2i}, \tag{6}$$

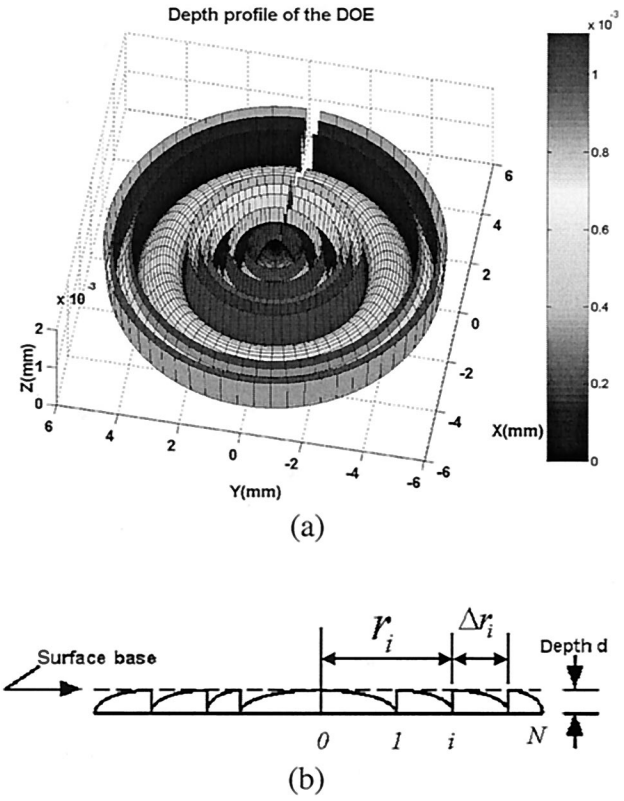

Fig. 9. (a) Depth profile of the DOE. (b) DOE parameters.

where $r_{\max}$ is the radius of the maximum zone transitions. The size of the zones Δr is computed by subtraction of the radii of two adjacent zone transitions. Because the OPD gradient starts at zero on axis and becomes steeper as it approaches the edge, the zones in the center are wide and become progressively finer near the edge. As the zones become finer, the diffraction efficiency drops off as predicted by scalar diffraction theory. Therefore DOE manufacturers recommend a limit on the minimum zone size. For example, the manufacturer of the lens recommended that the minimum zone size be no smaller than 15 μm. In the final design the radius of the DOE element $r_{\max}$ is 6.5 mm, the depth period d is 1.12 μm for a 550-nm wavelength, the minimum feature size is 74.65 μm, and the number of zones is 55.

5. Optimization

The system was optimized with rays traced from the pupil to the miniature display with CODE V (software from Optical Research Associates, Pasadena, Calif.) for a full unvignetted 12-mm pupil and a circular FOV of 52.4 deg. The design is rotationally symmetric, requiring optimization over only half of the FOV in one radial direction. During the process of optimization all the curvatures of the refractive surfaces, the distance between two adjacent surfaces, the coefficients of the aspheric substrate, and the DOE phase function were set as variables. The effective focal length was constrained to be 35 mm, and the quadratic coefficient of the DOE $c_q \geq -0.001$. The thickness of the components and the space among them were bound. The total thickness of the system was restricted in the last stage of the optimization for compactness. Five visual fields, 0, 0.2, 0.5, 0.7, and 1.0 (i.e., on axis, 7, 14, 21, and 26.2 deg, respectively), were optimized. The weighting of the five fields were adjusted during the optimization process. The final weighting was 1.0, 0.8, 0.8, 0.5, 0.3 for each field, respectively.

During the final optimization stage an aspheric surface was added to the first surface of the third plastic element to minimize the residual spherical and coma aberrations. Its profile function $Z_6(h)$ is described as

$$Z_6(h) = \frac{ch^2}{1 + [1 - (1 + k)c^2h^2]^{1/2}} + Ah^4 + Bh^6 + Ch^8 + Dh^{10} + Eh^{12}. \tag{7}$$

Coefficients k, c, A, B, C, D, and E were initially set to zero and were set to vary during optimization. In the final design $k = 1.0672497392$, $c = -0.062914$, $A = -0.7324993e^{-4}$, $B = 0.9704433e^{-5}$, $C = -0.74543809e^{-6}$, $D = 0.25956e^{-7}$, and $E = -0.346617e^{-9}$. To obtain the performance demonstrated in Section 6, we needed aspheric coefficients to as higher the 12th order. A further investigation could explore the degradation with fewer orders. However, from a fabrication point of view the only metric that matters is the final profile of the surface,

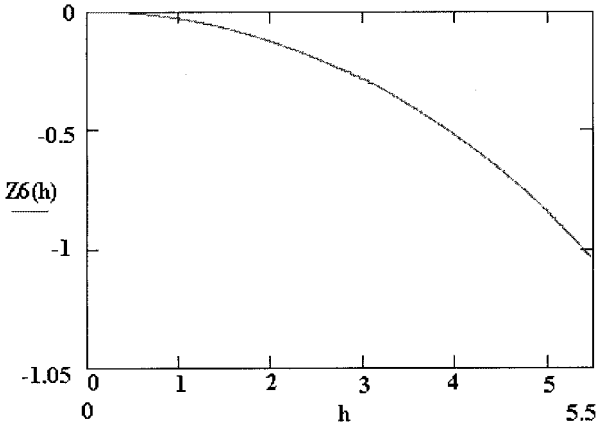

Fig. 10. Profile of the second aspheric surface.

which is shown in Fig. 10. The layout of the final design of the lens and the lens assembly are shown in Figs. 11(a) and 11(b), respectively. The lens performance is described in detail in Section 6.

6. Performance Evaluation

Since the improved axial performance of the design depends on the DOE surface, it is important to evaluate the diffraction efficiency of the DOE. Furthermore, as suggested by Shenker, the image quality of the HMDs is more informative when assessed in visual space.[30] A comprehensive framework for assessing a design in visual space and associated macrofiles are provided in Ha and Rolland.[31,32] At least three essential potential optical limitations encountered in the HMDs must be assessed: accommodation shift (i.e., defocusing across the FOV), astigmatism, and, for color displays, transverse chromatic smear. Therefore we evaluate the DOE in Subsection 6.A, an analysis of the optimized system when ray traced from the eye to the miniature display in Subsection 6.B, and the performance in visual space described in Subsection 6.C.

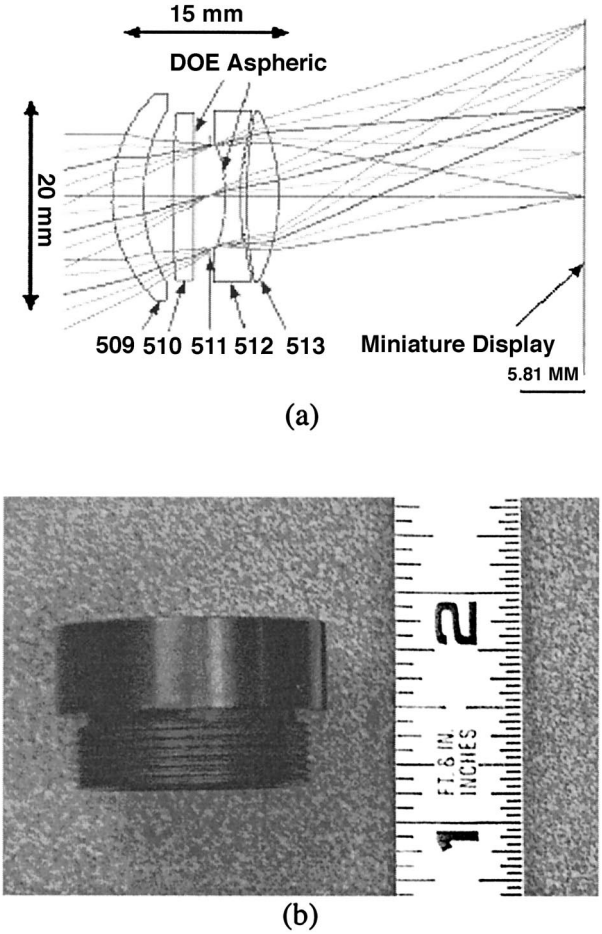

Fig. 11. Ultra-light projection lens for the HMPD: (a) lens layout and (b) lens assembly.

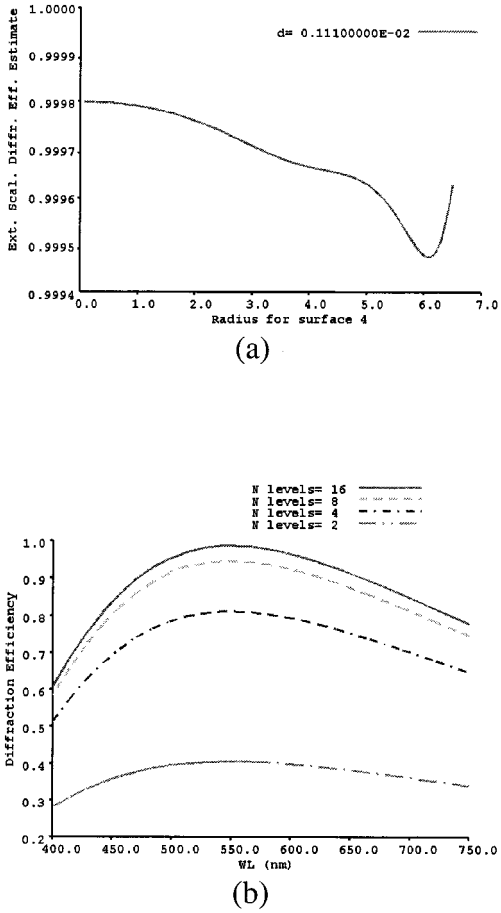

Fig. 12. Diffraction efficiency of the DOE: (a) diffraction efficiency across the radius and (b) diffraction efficiency versus wavelength.

A. Diffraction Efficiency of the Diffractive Optical Element

As predicted by scalar diffraction theory the diffraction efficiency of the DOE drops as its features become finer near the edge. The relationship of the diffraction efficiency across the radius for the designed wavelength (i.e., 550 nm) is shown in Fig. 12(a). Results show that there is a slight decrease across the radius, but the variation is extremely small, ranging from 0.9998 to 0.9995. Despite energy loss from the +1 order into the other orders,

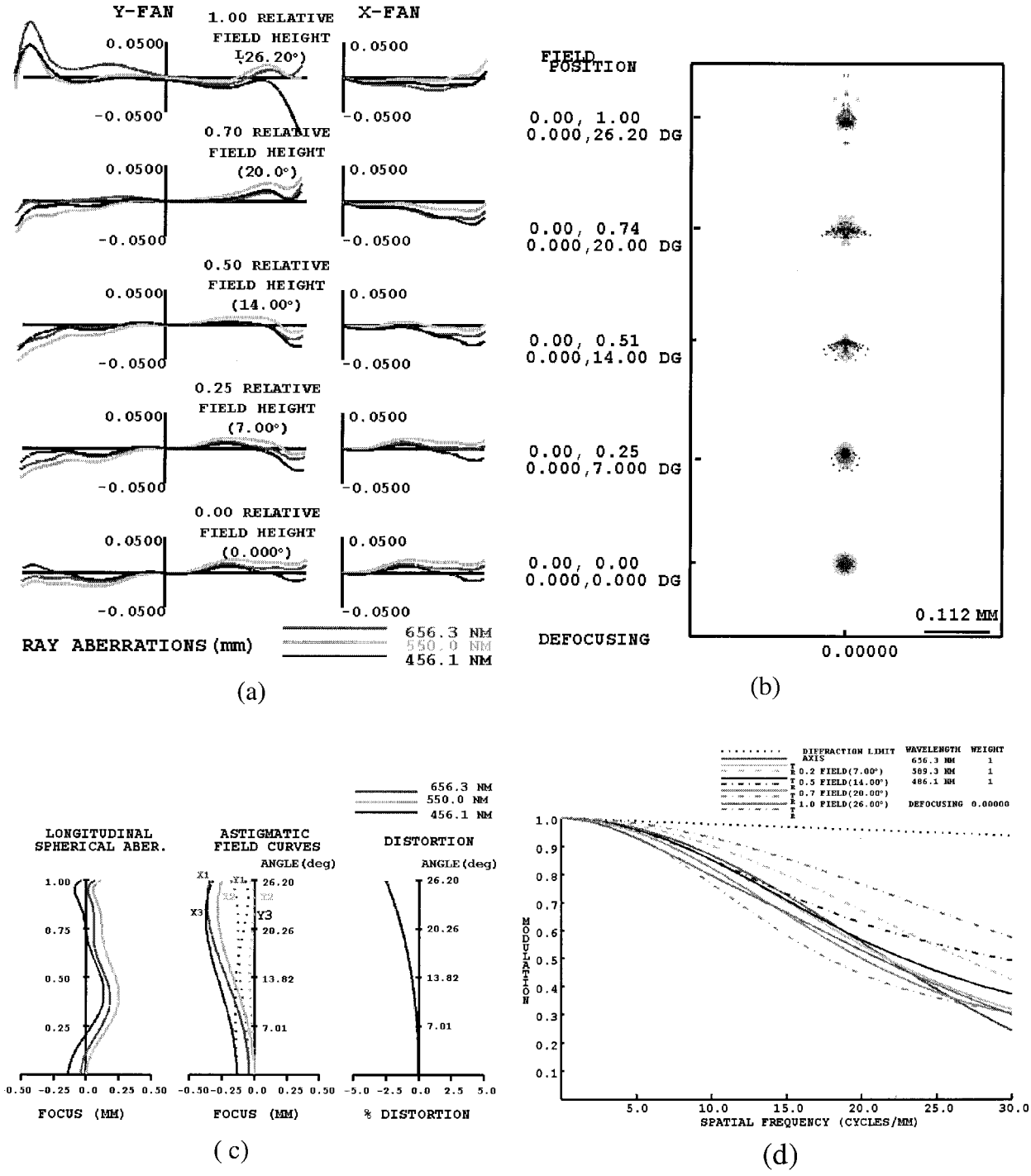

Fig. 13. Lens performance for the 12-mm, full-size pupil in object space: (a) Rayfan plot across the five field angles, (b) spot diagram across the five field angles, (c) astigmatism and distortion, (d) polychromatic MTF as a function of the spatial frequency in line pairs per millimeter.

because the amount is extremely small we anticipate no significant contribution to ghost images or degradation in the MTF.

The diffraction efficiency is wavelength dependent. Figure 12(b) shows the relationship of the diffraction efficiency as a function of wavelength as well as the levels of the binary masks (i.e., 2, 4, 8, 16). Results show that the efficiency variation ranges from 85% to close to 100% for the 16-level masks within the visible spectrum and decreases to 40% for the two-level masks. A large number of binary masks is typically used to predict the diffraction efficiency of the Kinoform DOEs. For example, 16 levels of binary masks lead to an accurate approximation.

B. Performance in the Miniature-Display Space

The various optical performances of the optimized lens is assessed first in the miniature-display space

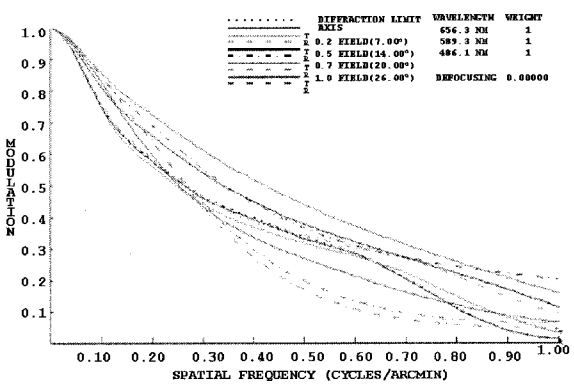

(a)

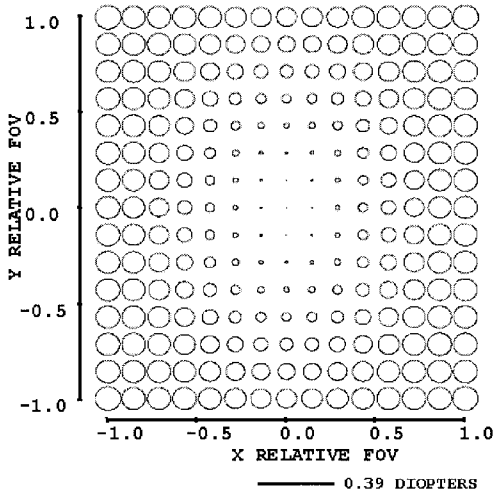

(b)

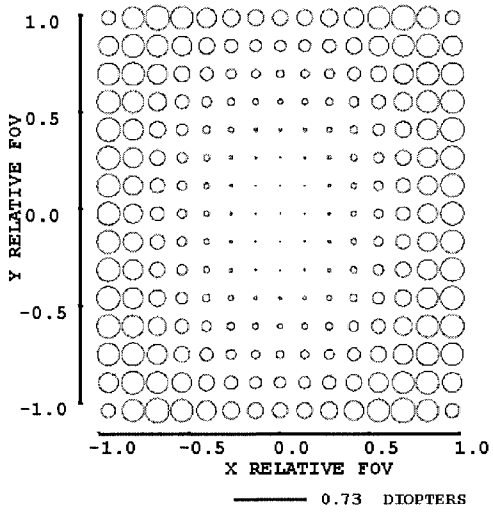

(c)

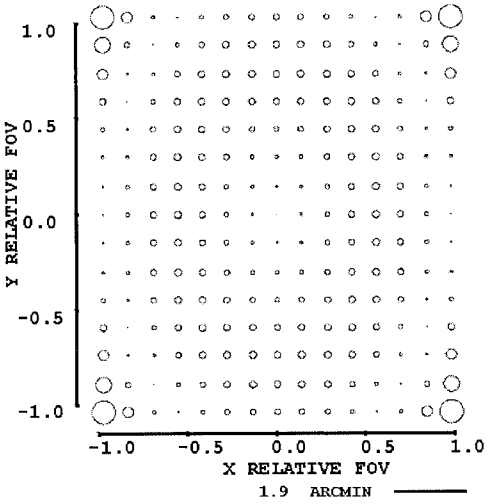

(d)

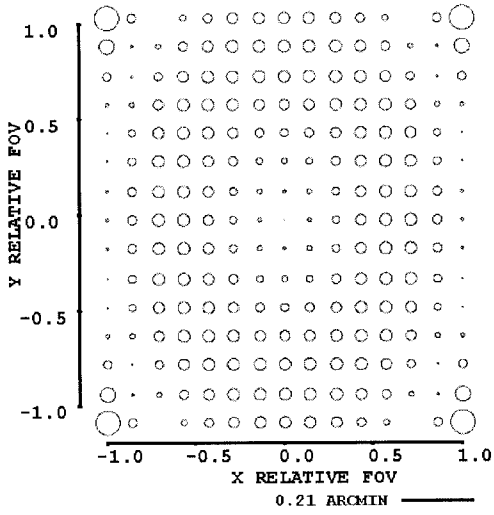

(e)

Fig. 14. Lens performance for a 3-mm centered pupil in visual space: (a) polychromatic MTF as a function of the spatial frequency in cycle per arc minutes; (b) accommodation versus display location (DOF diopter range, −0.35–0.35, acceptable acuity 3 arc min); (c) astigmatism versus display location (DOF diopter range, −0.35–0.35, acceptable acuity 3 arc min); (d) transverse lateral color versus display location; (e) transverse second color versus display location.

across the five representative field angles for three wavelengths (656.3, 550, and 456.1 nm). A 12-mm full-size pupil is considered in this analysis.

The rayfan plots and the spot diagrams are shown in Figs. 13(a) and 13(b), respectively. We observe residual higher-order coma in the design. The spot diagrams demonstrate the overall high performance of the design with a maximum rms spot diameter of 0.03 mm that is smaller than the pixel size (i.e., 0.042 mm) of the LCD display.

The primary aberrations including longitudinal spherical aberration, astigmatism, and distortion are shown in Fig. 13(c) for a 12-mm pupil. The maximum spherical aberration occurs at 0.4 in the aperture. The performance shows that the residual astigmatism is well balanced over the entire FOV. The residual astigmatism reaches a maximum of 0.25 mm at a 21-deg FOV. Distortion of the system is well corrected and less than 2.5% across the overall FOV.

The polychromatic diffraction MTF for the full 12-mm pupil is presented across the five representative field angles, as shown in Fig. 13(d). The target LCD display (see Table 1) has a spatial frequency of 25-lp/mm given a 42-μm pixel size. Note that the modulation ratio of the design presented at 25-lp/mm is ~45% across the FOV. Therefore the performance is currently limited by the miniature-display resolution.

C. Performance in Visual Space

To help bridge the gap between the optical-design engineers and the perceptual scientists, we provide an assessment of the design in visual space in terms of the polychromatic MTF expressed in cycles per arc minute, accommodation shift and astigmatism expressed in diopters, and color smear expressed in arcminutes, adopting the metrics first proposed by Shenker for HMDs[30] and further expanded on by Ha and Rolland.[31,32] We utilized the macrofiles provided on the ODALab website, http://odalab.ucf.edu/macro.

The optical system is inverted first and a perfect lens is inserted into the exit pupil to bring the image into focus. A 3-mm centered pupil is assumed in all analyses pertaining to the visual performance presented. Visual acuity is estimated to be 3 are min, the limit imposed by the resolution of the LCD displays.

Using the macro VSMTF.seq, we insert a perfect lens of 421.47-mm focal length on the surface of the exit pupil, and the polychromatic diffraction MTFs shown in Fig. 14(a) are plotted against the spatial frequency to as great as 1 cycle/arc min. The MTF presents ~45% modulation at 0.3 cycle/arc min (i.e., 1 cycle/3 arc min). While the LCD display currently limits visual acuity in an HMD to 3 arc min, the lens itself can support higher-resolution miniature displays: The MTF presents ~40% modulation at 0.5 cycle/arc min (i.e., 1 cycle/2 arc min or 2-arc min resolution) and 20% modulation at 0.8 cycle/arc min (i.e., 1 cycle/1.25 arc min or 1.25-arc min resolution). Thus the lens performance basically matches the visual acuity of the human visual system.

The accommodation shift is measured with respect to the center position of the sagittal and tangential foci across the FOV. Figures 14(b) and 14(c) are obtained with the macro VSCAS.seq with a 17-mm perfect lens inserted on the surface of the exit pupil. They show the accommodation shift and the astigmatism across the FOV in diopters. The plots are generated such that circles are displayed only for points whose defocus falls within the depth of focus of the human visual system for the virtual image distance. The diameter of the circle in the plot is proportional to the magnitude of the accommodation shift and astigmatism. Results show that all points in the FOV fall within the depth of focus of the human visual system around the nominal focus, and thus all points in the FOV will be perceived sharply and as points (not lines as perceived for astigmatism exceeding the tolerance of the human visual system).

The transverse lateral color and secondary color smear, computed in arc minutes with VSTCS.seq, are shown in Figs. 14(d) and 14(e), respectively. Results show that, based on a 3-arc min resolution, the lens is limited neither by accommodation, astigmatism, nor a color smear. Other analyses with the same macros but with different levels of resolution could be conducted to as high as the resolution of the human visual system. While a complete analysis of the lens in visual space to as high as a 1-arc minute resolution is not presented in this paper, some of the results on the MTF to as high as 1 cycle/arc min indicate that the lens basically matches the performance of the human visual because the lens enables ~1.25-arc min resolution. The lens was built and successfully integrated in the HMPD prototype whose comprehensive design and assessment are being prepared for publication.

7. Conclusion

We have presented the conception, optimization, and assessment of an ultralight and compact projection lens by using the combination of a diffractive optical element, plastic components, and aspheric surfaces for a new generation of HMPD prototypes. The analysis of the lens with respect to the miniature display shows that the latter currently limits the resolution to 3 arc min. The analysis with respect to the MTF in visual space to as high as 1 cycle/arc min demonstrates that the lens can provide an ~1.25-arc min resolution.

We thank Joachim Bunkenburg of the former Rochester Photonic Corporation and Rick Plympton of Optimax Corporation for generous assistance with the lens fabrication. We thank Chunyu Gao for help in designing the lens assembly. The HMPD system was supported by National Science Foundation (NSF) grants IIS 00-83037 ITR and IIS 00-82016 ITR, the Media Interface and Network Design Lab at Michigan State University, and the NSF EIA-99-86051. The research was also supported by the Na-

tional Institutes of Health/National Library of Medicine grant 1-R29-LM06322-01A1, and the ELF Corporation.

References

1. W. Barfield and T. Caudell, eds., *Fundamentals of Wearable Computers and Augmented Reality* (Lawrence Erlbaum Associates, Mahwah, N.J., 2001).
2. D. Buxton and G. W. Fitzmaurice, "HMDs, caves, and chameleon: a human-centric analysis of interaction in virtual space," *Computer Graphics* (Association for Computing Machinery, New York, 1998), Vol. 32, No. 4, pp. 69–74.
3. J. P. Rolland, D. Ariely, and W. Gibson, "Towards quantifying depth and size perception in virtual environments," *Presence: Teleoperators and Virtual Environments* (MIT, Cambridge, Mass., 1995), Vol. 4, No. 1, pp. 24–49.
4. A. State, G. Hirota, D. T. Chen, W. E. Garrett, and M. Livingston, "Superior augmented-reality registration by integrating landmark tracking and magnetic tracking," in *Proceedings of the ACM SIGGRAPH Conference on Computer Graphics 1996* (Association for Computing Machinery, New York, 1996), pp. 429–438.
5. J. P. Rolland and H. Fuchs, "Optical versus video see-through head-mounted displays in medical visualization," *Presence: Teleoperators and Virtual Environments* (MIT, Cambridge, Mass., 2000), Vol. 9, No. 3, pp. 287–309.
6. R. Kijima and T. Ojika, "Transition between virtual environment and workstation environment with projective head-mounted display," in *Proceedings of the IEEE 1997 Virtual Reality Annual International Symposium* (IEEE Computer Society, Los Alamitos, Calif., 1997), pp. 130–137.
7. J. Fergason, "Optical system for head mounted display using retroreflector and method of displaying an image," U.S. patent 5,621,572 (15 April 1997).
8. C. Cruz-Neira, D. J. Sandin, and T. A DeFanti, "Surround-screen projection-based virtual reality: the design and implementation of the CAVE," in *Proceedings of the ACM SIGGRAPH 93* (Association for Computing Machinery, New York, 1993), pp. 135–142.
9. J. Parsons, and J. P. Rolland, "A nonintrusive display technique for providing real-time data within a surgeons critical area of interest," in *Proceedings of Medicine Meets Virtual Reality98*, (IEEE Computer Society, (Los Alamitos, Calif., 1998), pp. 246–251.
10. H. Hua, A. Girardot, C. Gao, and J. P. Rolland. "Engineering of head-mounted projective displays," Appl. Opt. **39,** 3814–3824 (2000).
11. H. Hua and J. P. Rolland, "Compact lens-assembly for wearable displays, projection systems, and cameras," U.S. patent application, 60–292, 942 (23 May 2001).
12. H. Hua, C. Gao, F. Biocca, and J. P. Rolland, "An ultralight and compact design and implementation of head-mounted projective displays," in *Proceedings of IEEE-VR 2001* (IEEE Computer Society, Los Alamitos, Calif., 2001), pp. 175–182.
13. F. Biocca and J. Rolland, "Teleportal face-to-face system," U.S. patent application 6550-00048 (22 December 2000).
14. N. Kawakami, M. Inami, D. Sekiguchi, Y. Yangagida, T. Maeda, and S. Tachi, "Object-oriented displays: a new type of display system—from immersive display to object-oriented displays," in *Proceedings of IEEE International Conference on Systems, Man, and Cybernetics'99* (IEEE Computer Society, Los Alamitos, Calif., 1999), Vol.5, pp.1066–1069.
15. H. Hua, C. Gao, L. Brown, N. Ahuja, and J. P. Rolland. "Using a head-mounted projective display in interactive augmented environments," in *Proceedings of IEEE and ACM International Symposium on Augmented Reality 2001* (Association for Computing Machinery, New York, 2001), pp. 217–223.
16. H. Hua, C. Gao, L. Brown, N. Ahuja, and J. P. Rolland, "A testbed for precise registration, natural occlusion, and interaction in an augmented environment using a head-mounted projective display (HMPD)," in *Proceedings IEEE VR 2002* (IEEE Computer Society, Los Alamitos, Calif., 2002), pp.81–89.
17. M. Inami, N. Kawakami, D. Sekiguchi, Y. Yanagida, T. Maeda, and S. Tachi, "Visuo-haptic display using head-mounted projector," In *Proceedings of IEEE Virtual Reality 2000* (IEEE Computer Society, Los Alamitos, Calif., 2000), pp.233–240.
18. J. P. Rolland, J. Parsons, D. Poizat, and D. Hancock, "Conformal optics for 3D visualization," in *International Optical Design Conference 1998*, L. R. Gardner and K. P. Thompson, eds., Proc. SPIE 3482, 760–764 (1998).
19. R. E. Fischer, "Optics for head-mounted displays," Inf. Displ. 10, No. 7–8, 12–16 (1994).
20. I. P. Howard and B. J. Rogers. *Binocular Vision and Stereopsis*, Oxford Psychological Series 29 (Oxford University, New York, 1995).
21. D. F. Kocian and H. L. Task, "Measurement of military helmet and head-mounted display (HMD) visor optical properties," in *Helmet- and Head-Mounted Displays V*, R. J. Lewandowski, L. A. Haworth, and H. J. Girolamo, eds., Proc. SPIE **4021,** 120–132 (2000).
22. J. Bunkenburg and T. A. Fritz, "Innovative diffractive eyepiece for a helmet-mounted display," *Novel Optical Systems and Large-Aperture Imaging*, K. D. Bell, M. K. Powers, and J. M. Sasian, eds., Proc. SPIE **3430,** 41–49 (1998).
23. H. Ogawa, "Optical system with refracting and diffracting optical units, and optical instrument including the optical system," U.S. patent 5,930,043 (27 July 1999).
24. J. B. Caldwell, "Diffractive apochromatic double-Gauss lens," Opt. Photon. News (October 1999), pp. 43–45.
25. C. W. Chen, "Application of diffractive optical elements in visible and infrared optical systems," in *Lens Design*, W. J. Smith, ed., SPIE Critical Reviews Series CR41 (Society of Photo-Optical Instrumentation Engineers, Bellingham, Wash., 1992), pp. 158–172.
26. "Holographic and diffractive optical elements," *Optical Research Associate Course Notes* (Pasadena, Calif., 1999).
27. M. W. Farn and W. B. Veldkamp, "Binary optics," in *Handbook of Optics*, Vol. 2 Devices, Measurements, and properties, M. Bass, ed. (McGraw-Hill, New York, 1995).
28. D. C. O'Shea, *Elements of Modern Optical Design* (Wiley, New York, 1985).
29. W. Knapp, G. Blough, K. Khajurivala, R. Michaels, B. Tatian, and B. Volk, "Optical design comparison of 60° eyepieces: one with a diffractive surface and one with aspherics," Appl. Opt. **36,** 4756–4760 (1997).
30. M. Shenker, "Optical design criteria for binocular helmet-mounted displays," in *Display System Optics*, A. Cox and R. Hartmann, eds., Proc SPIE **778,** 70–78 (1987).
31. J. P. Rolland. "Wide-angle, off-axis, see-through head-mounted display," Opt. Eng. **39,** 1760–1767 (2000).
32. Y. Ha and J. P. Rolland, "Optical assessment of head-mounted displays in visual space," Appl. Opt. **41,** 5282–5289 (2002).